Arch. Metall. Mater. **63** (2018), 1, 173-180

DOI: 10.24425/118925

S. WEISS*,**#, I. RIEHL*, J. HANTUSCH**, U. GROSS*

NUMERICAL INVESTIGATION ON THE CRUCIBLE DISCHARGE OF STEEL AND SLAG DURING THE ALUMINOTHERMIC WELDING PROCESS

The aluminothermic reaction is a type of self-propagating high-temperature synthesis to produce high quality metals and metal oxides en route. The main use of the aluminothermic reaction is in the field of railway welding. The multiphase flow of steel, slag and air in differently shaped crucibles has been numerically investigated in this work with the volume-of-fluid method. The simulations were carried out with the multiphase solver of the open source toolbox OpenFOAM. To validate the numerical results of the three-dimensional simulations, an experiment was carried out to investigate the discharge of a water-oil system from the crucible. A comparison to a numerical 3D simulation showed reasonable accurate results. It can be said that the solver is capable of predicting the point of the oil penetration of the water phase in the experiment.

Keywords: aluminothermic reaction; thermite; SHS; VOF; OpenFOAM

1. Introduction

For the process of railway welding, the aluminothermic (AT) reaction is used to produce liquid steel at high temperatures directly at the construction site in short amounts of time and of the desired quality and composition. Thermite, a powder composite made of aluminium (Al) and iron(III) oxide (Fe_2O_3), was introduced by the patent from [7] and since its first mention in 1895 it has been used for the AT reaction. The underlying chemical conversion can be expressed by the exothermic redox reaction in equation (1). The standard enthalpy of reaction ΔH_R^0 is negative due to the dissipation of heat to the environment during the reaction

$$Fe_2O_3 + 2Al \rightarrow 2Fe + Al_2O_3,\ \Delta H_R^0 < 0 \qquad (1)$$

For simplification reasons no partial reactions, intermetallic products and alloying elements are included in equation (1). Thermite is ignited inside a crucible and during the reaction the propagation front travels through the crucible at velocities in the range 1 – 10 mm/s. In the reaction zone, apart from chemical reactions, thermal diffusion, convection and radiation, a volume and density change occurs due to the conversion of the species, followed by the separation of liquid phases in the gravitational field. The outlet of the crucible opens automatically after a certain amount of time and liquid steel and slag discharges into the mould, which is positioned underneath.

In the scope of this research, numerical simulations of the discharge process have been carried out to investigate a three-phase system of steel, slag and air in two types of crucibles as shown in Fig. 1. The position at $x = 0$ m represents the centreline and the radius R is equal to the maximum crucible radius. A water-oil experiment was used for validation of the numerical algorithm.

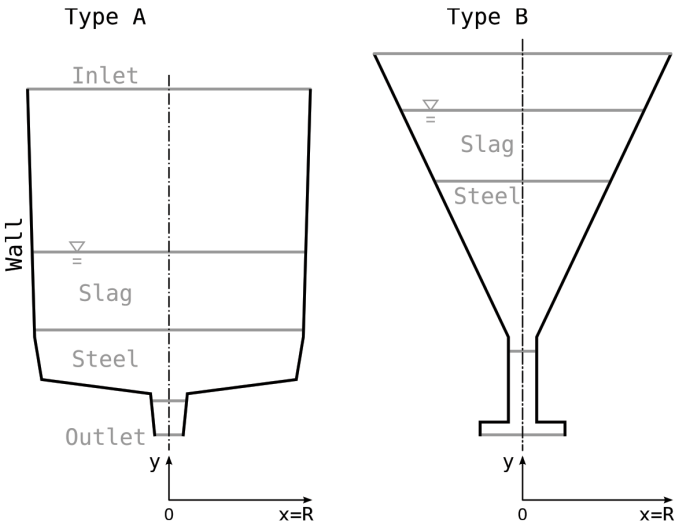

Fig. 1. Schematic internal contour including the approximate initial position of the interfaces in the two types of crucibles used in the 2D and 3D numerical simulations

Type A is a one-time-use crucible and B is used for multiple weldings. Both crucibles differ in wall geometry and material. Type A is made of waterglass-bonded silicium oxide and B of

* TU BERGAKADEMIE FREIBERG, FREIBERG, GERMANY
** GOLDSCHMIDT THERMIT GMBH, LEIPZIG, GERMANY
# Corresponding author: sebastianw@posteo.de

a waterglass-bonded aluminium-silicium oxide composite, which shows greater thermal resistance against the melt temperatures due to the aluminium oxide (Al_2O_3) content compared to the pure silicon oxide (SiO_2) material.

Many numerical investigations in the field of multiphase steel-slag-air systems have been carried out for the continuous casting process [1,8,13] in which melt temperatures are below 2000°C. The thermophysical properties of steel differ to a certain degree, making a direct comparison of numerical results complicated. The turbulent nature of the multiphase flow in the area of the submerged entry nozzle (SEN) causes slag from the surface to be entrained into the steel. Another study on the topic of slag entrainment has been made in [16] and [17]. In [17] the numerical results have been validated against the results of a water-oil experiment. Slag entrainment occurs also during the teeming of ladles [15]. Research has shown that the critical height of the slag funnel formation is, amongst others, depending on the ratio of ladle to outlet diameter.

2. Methods

The simulations were carried out with the volume-of-fluid (VOF) solver *multiphaseInterFoam* of the open source CFD (Computational Fluid Dynamics) tool kit OpenFOAM. This solver is capable of simulating incompressible, isothermal *n*-phase systems using a volume-of-fluid approach [10]. Thermophysical properties for the three-phase system have been found in literature and more complex data has been calculated by empirical formulations. An experiment has been used for the validation of solver and numerical schemes by recording the outflow of an immiscible water-rapeseed oil system from the original type A crucible. A mesh independence study was also conducted on both crucibles A and B of the steel-slag system, in which the volume flow rate at the outlet has been compared between three two-dimensional meshes, varying in cell size, respectively.

The multiphase flow inside the crucible is gravity driven and the phases are at rest in the initial state. Maximum flow velocities $\vec{u}$ are reached in the narrowest passage of the diameter d. The investigation of the flow type, laminar or turbulent, in the crucible was not easily distinguishable especially for the multiphase system.

Due to the fact that the kinematic viscosity is different for each phase, one can estimate that the maximum Reynolds number at constant phase velocities is present in the phase having the smallest viscosity value. Liquid steel has the lowest kinematic viscosity of the phases and in the narrowest cross section the Reynolds number will reach values above the critical value for pipes in both crucibles. Hence, the flow is highly turbulent near the outlet.

Due to the obvious turbulent nature of the flow at the outlet region, the standard k-ε turbulence model was used in the simulations. Moreover, the model was validated against the experimental results from the water-oil experiment. By comparing the numerical results to the water-oil experiment, namely the point in time for the oil breakthrough of the water phase, only the standard k-ε turbulence model was able to predict a parallel outflow of the two liquid phases accurately.

3. Governing equations

The *n*-phase solver *multiphaseInterFoam* is based upon the two-phase, isothermal, incompressible, volume-of-fluid algorithm *interFoam* [14] for which conservation of mass is expressed through the continuity equation (2) and conservation of momentum for a single phase fluid (3), reading

$$\nabla \cdot \vec{u} = 0 \tag{2}$$

$$\frac{\partial(\rho\vec{u})}{\partial t} + \nabla\cdot(\rho\vec{u}\vec{u}) = -\nabla p + \nabla\cdot\tau + \int_{S(t)} \sigma\kappa' \mathrm{n}'\delta(x-x')\mathrm{d}S + \overrightarrow{f_{ex}} \tag{3}$$

The left hand side of equation (3) contains the transient as well as the advective transport of the fluid element. The right hand side of equation (3) includes pressure ∇p and friction forces $\nabla \cdot \tau$ with the stress tensor τ and the dynamic viscosity μ, which can be described by equation (4)

$$\tau = \mu(\nabla\vec{u} + \nabla\vec{u}^T) \tag{4}$$

The integral of a three-dimensional δ – function in equation (3) represents the momentum source due to a surface tension force acting in normal direction n on the surface of the interface $S(t)$, which is a function of the time t. The notation ()' represents hereby a value directly on the interface, e.g. κ' being its curvature. Gravitational body forces $\rho\vec{g}$ acting on the fluid element are external forces considered in $\overrightarrow{f_{ex}}$ in equation (3).

4. Volume-of-fluid method

In the VOF method, being a volume tracking method, an indicator function is introduced for the tracking of the interface by the phase fraction φ. Here, the convection scheme for φ has to guarantee to remain bounded between zero and unity, according to [14]. Other numerical methods for two-phase flows can be divided into surface tracking, mesh moving or volume tracking, which includes also, besides VOF, level-set and phase field algorithms [14].

The surface force term in equation (3) is approximated by the continuum surface force approach (CSF) [2], see equation (5), with κ as the surface curvature, the surface tension σ and the gradient of the phase fraction φ reading

$$\int_{S(t)} \sigma\kappa' \mathbf{n}'\delta(x-x')\mathrm{d}S \approx \sigma\kappa\nabla\varphi \tag{5}$$

$$\kappa = \nabla\cdot\left(\frac{\nabla\varphi}{|\nabla\varphi|}\right) \tag{6}$$

Based upon the evaluation of an indicator function, in the VOF method such an indicator is the phase fraction φ within a range of zero and unity for a two-phase system.

$$\varphi = \begin{cases} 1, \ \textit{fluid A} \\ 0 < \varphi < 1, \ \textit{interfacial region} \\ 0, \ \textit{fluid B} \end{cases}$$

The φ transport is expressed through equation (7) by a transient, convective and artificial compression term with the compression velocity $\overrightarrow{u_r}$

$$\frac{\partial \varphi}{\partial t} + \nabla \cdot (\vec{u}\varphi) + \nabla \cdot (\overrightarrow{u_r}\varphi(1-\varphi)) = 0 \tag{7}$$

The compression term $\nabla \cdot (\overrightarrow{u_r}\varphi(1-\varphi))$ is zero within fluid domains where φ = [0,1]. However, in a thin interfacial region unequal zero and there it is used for the reduction of the interfacial width [14]. The phase fraction φ is used to track the interface, segregating the phases and since the VOF method is a pseudo one-fluid approach, φ is needed for the calculation of the local thermophysical properties, e.g. density ρ and dynamic viscosity μ in equation (8) and (9)

$$\rho = \phi\rho_A + (1-\phi)\rho_B \tag{8}$$

$$\mu = \phi\mu_A + (1-\phi)\mu_B \tag{9}$$

The difficulty of the accurate numerical simulation with the VOF model lays within the approximation of surface tension force term in equation (3), the tracking and reconstruction of the interface over the time *t*, according to [14].

The OpenFOAM implementation of the VOF method uses a modified flux corrected transport method (FCT) called MULES (Multidimensional Universal Limiter for Explicit Solution) and it is based upon the work of [19] with an iterative calculation of the weighting factors [4]. For further reading on MULES see the work of [4].

The pressure-velocity coupling is being carried out by the PISO (Pressure Implicit with Splitting of Operators) algorithm, including a momentum predictor from the previous time step [4] and corrector loop amongst others, which solves the pressure equation and correcting the momentum equation based upon the pressure change [14].

Furthermore, the reconstruction of the interface in OpenFOAM is carried out by the MULES algorithm. PLIC (Piecewise Linear Interface Construction) is another common method used in CFD.

5. Boundary conditions

A temperature of the melt T_{melt} = 2473K will be used as an estimate after completion of the thermite reaction. This value is used to appraise the thermophysical properties of the melt. The OpenFOAM multiphase VOF solver does not account for energy transport in the flow and therefore the solver uses constant hydrodynamic properties.

The densities were linear extrapolated yielding 6540 kg/m^3 and 3740 kg/m^3 for low-alloyed steel melt and slag respectively. The dynamic viscosity η of steel amounts to 5×10^{-3} Pa/s [8], [9], [11]. The slag consists, depending on the crucible, mainly of Al_2O_3, Fe_2O_3, SiO_2 and to a low extend MnO and other oxide residues. The dynamic viscosity of the slag can be estimated with Ray's model [5] yielding 0.2273 Pa/s.

Volumes of steel and slag inside the crucibles have been calculated using the initial mass of a special thermite portion of 13.6 kg, the estimated density at T_{melt} and the mass fraction of the products which accounts to 0.56 and 0.44 for steel and slag respectively. It is assumed that the yield of steel and slag accounts to 7.616 kg and 5.984 kg respectively.

Both crucibles contain different air volumes above the slag and to a low extent at the outlet below the steel phase. To estimate the proper reference temperature for the thermophysical properties of the air, a simulation of the convective heat transfer from the slag surface to the air volume V was carried out. This simulation was run for a physical duration of 10 s for both crucibles. The average air temperature $\overline{T}$ was then calculated by equation (10)

$$\overline{T} = \frac{1}{V}\int_V T \mathrm{d}V \tag{10}$$

This yields an average air temperature of 1083.2 K and 2200 K for crucibles A and B respectively. The difference in both temperatures is due to the fact that a much smaller volume of air is enclosed in B than in A. Therefore, the air volume can heat up much faster by convection and conduction during the given time period. In this context the transport of thermal energy by radiation from the slag surface to the air was not investigated.

The dynamic viscosity of air inside the crucibles can be estimated for the type A and B crucibles to be 4.3788×10^{-5} Pa/s and 6.8421×10^{-5} Pa/s respectively. The surface tension of the Al_2O_3 slag was obtained as 577.039×10^{-3} N/m following [12]. In [12], it is stated that the surface tension of steel is primarily influenced by the weight percent of oxygen and sulphur. However, the formulation also includes the weight percent of carbon and the temperature of the melt. The surface tension of steel will therefore be assumed to be 1.5772 N/m. The interfacial tension is of interest since the present multiphase system consists of three phases, namely two liquid and one gaseous phase. It will be assumed that air has no influence on the surface tension of steel and slag. In the actual process, however, air is known to reduce the surface tension of liquid steel through oxidation. The interfacial tension between metal and slag is calculated [6] and yielding 1.2 N/m. Correlating with interfacial tension measurements of a Fe – Al_2O_3 system [18] and by considering the surface activity of atmospheric oxygen and its ability to reduce the surface tension in steel [3], the value obtained from [6] is reasonable.

The contact angle between the phases and the crucible wall was assumed to be 90° since no experimental data of liquid steel and slag on waterglass-bonded Al_2O_3 and SiO_2 materials was available. Also the interfacial contact angle at the three-phase region of the system steel-slag-air was assumed to be 90°.

6. Numerical validation with water-oil system

In this section the experimental results of the water-oil outflow from the type A crucible for the validation of the numerical algorithms is presented. For the experimental setup, as shown in Fig. 2, crucible A was investigated due to the fact that the parallel outflow of steel and slag over a distinguishable amount of time was found in the numerical simulations. Hence, the experimental setup of the discharge of water and oil is based upon geometrical similarity by using an original type A crucible. Furthermore, the fluid volume of water and rapeseed oil equates to that of liquid steel and slag respectively. Therefore, the geometric similarity of the fluid system could be guaranteed.

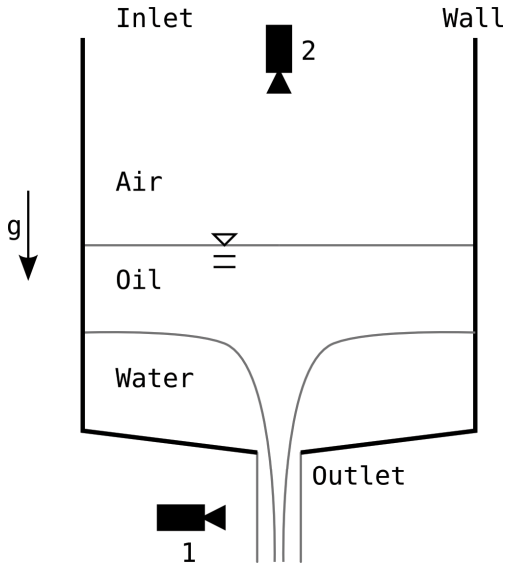

Fig. 2. Schematic concept of the experimental investigation and approximate positions of the two cameras

As an initial condition the three-phase system is completely separated and at rest. Water and rapeseed oil were used in the experiment. The density of the oil amounts to 912 kg/m^3. For better distinction between oil and water phases, the oil was pigmented through food colouring. Camera 1 is used to record the complete discharge process of the water-oil system and to detect the point in time for the oil penetration of water and the beginning of the parallel outflow of the two phases. Camera 2 recorded the surface flow direction on the oil surface.

However, numerical and experimental results have shown that the multiphase system behaves as a potential-flow structure in which the flow direction always points to the centre. The water-oil experiment was then numerically investigated for the type A crucible with the results displayed in Fig. 3.

Two points in physical time were of interest for the validation with experimental data, as seen in Fig. 4. The first corresponds to the breakthrough of oil through the water phase, yielding 0.64 s, and the second one is obtained at the end of the outflow, yielding 7.2 s, namely when air droplets can be seen in the oil stream. At this point, the phase fraction of oil will decrease below unity as the phase fraction of water is zero and that of air

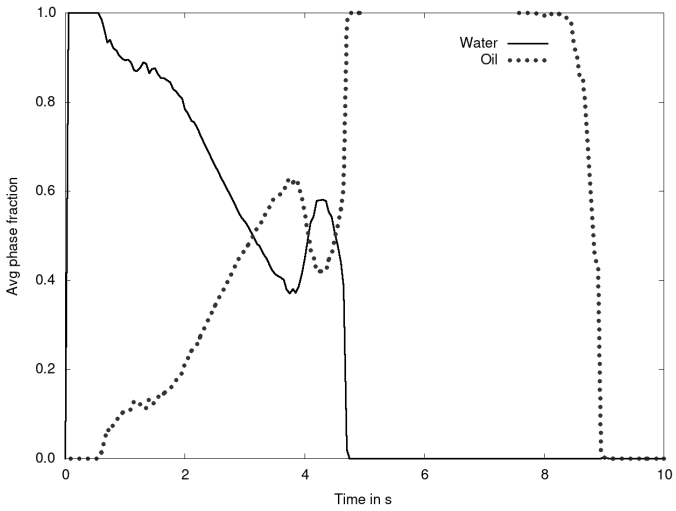

Fig. 3. Average phase fraction at the outlet of type A crucible based on the numerical simulation of the outflow of the water-oil system as a result of a three-dimensional numerical simulation

is greater than zero. Numerical results of the outflow of a water-oil multiphase system from type A crucible are shown in Fig. 3 for comparison. The point in time for the oil breakthrough in the numerical simulation yields 0.55 s with an absolute error of –0.09 s, as seen by a decreasing water phase fraction below unity. In the experimental validation, the oil breakthrough corresponds to a physical time of 0.64 s, as seen in frame B in Fig. 4. The outlet of the crucible is reached prior to this since the outlet is positioned above the field of view in Fig. 4. Therefore, we cannot make an exact quantification of the time for which the oil phase reaches the outlet. The most reliable data however correlates to 0.64 s in time frame B of Fig. 4.

The end of the discharge was reached at 7.9 s, according to the simulation. Comparing this value to the experiment, an absolute error of 0.7 s is obtained. These two numerical values depict the experimental results in a reasonable accurate way. Due to the experimental setup, the end time of the oil outflow could not be determined and therefore no comparison could be made.

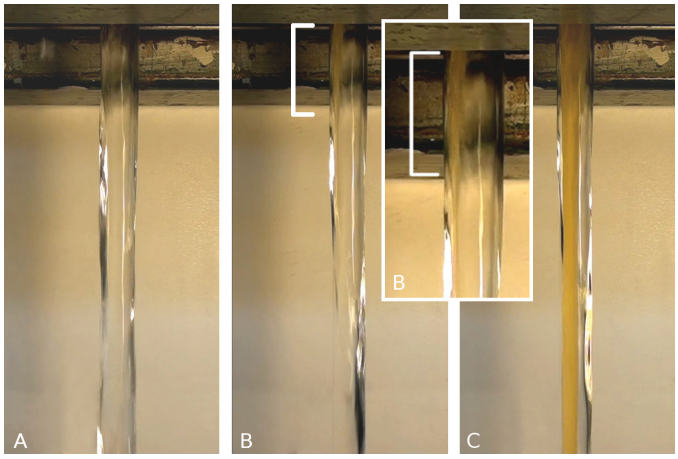

Fig. 4. Significant time frames A, B and C of the water-oil experiment in the type A crucible. The white square bracket represents the approximate length of the oil stream in the water, corresponding to physical times of 0.16 s, 0.64 s and 1.12 s respectively

Examining the results of the numerical simulation and experiment at significant times of the crucible discharge, we have observed that the VOF solver *multiphaseInterFoam* is capable of predicting the time for the oil penetration of water with minimal absolute error. During the parallel outflow of both phases, the solver is able to show the exact phase distribution in the stream as seen in the experiment, in particular when oil is being completely surrounded by the more dense water phase.

Fig. 4 shows selected time frames during the outflow in the water-oil system where A, B and C corresponds to a physical time of 0.16 s, 0.64 s and 1.12 s respectively. In B, the oil penetration of water occurs. In frame A of Fig. 4 only the water phase is visible and thus representing a physical time prior 0.55 s of the numerical results in Fig. 3 with the oil phase fraction being zero. In frame B of Fig. 4, the vertical length of the oil phase in the water stream at 0.64 s is indicated by a white bracket. Frame C of Fig. 4 relates to a time in between oil breakthrough and end of water outflow at approximately 4 s as shown in Fig. 3 with both liquid phases being present in the stream.

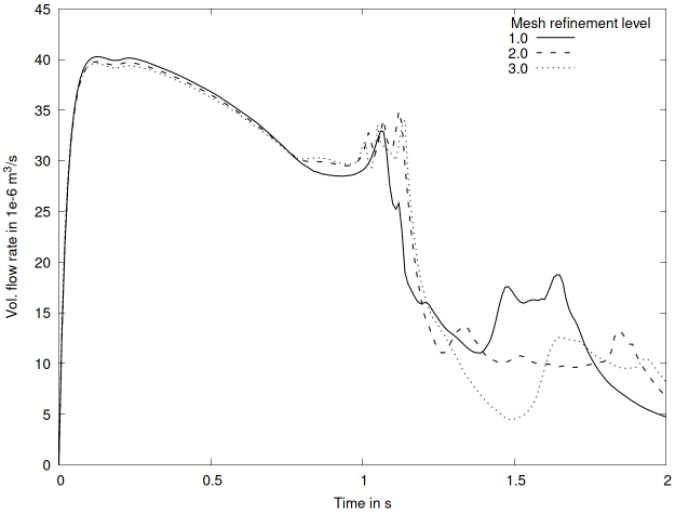

Fig. 5. Volume flow rate for the two-dimensional mesh independence study at the outlet of type A crucible during discharge for three mesh refinement levels

7. Numerical results for the steel-slag system

A two-dimensional study on the mesh independence for crucible A and B is shown in Fig. 5 and 6 respectively. In this evaluation the degree on which the 2D numerical solution is dependent on the cell size has been investigated. The block structured grid has been constructed by using the meshing tool *blockMesh*. Furthermore, the grid topology has been kept constant throughout the refinement process. Only the number of cells per block has been modified. The volume flow rate at the crucible outlet has been investigated for three refinement levels of a 2D computational mesh. Level 1 equates the cell count in a planar cross section of the 3D crucibles type A and B. In refinement levels 2 and 3, the number of cells has been doubled and tripled respectively. Comparing the volume flow rate over the discharge time for type A in Fig. 5, the variation in the flow rate before 0.75 s is minimal. By using a refinement level of 3, a decrease of 2×10^{-6} m^3/s and at 1 s an increase of similar magnitude is observable. The end of the outflow is initialized by a local maximum in the volume flow rate of 35×10^{-6} m^3/s at 1 s and with increasing refinement level these local maxima appear delayed. However, the magnitude of the local maximum is not affected by the refinement. The end of the discharge of the two-dimensional type A crucible is insignificant for 3D simulations. More important is the point in time for the phase change between steel and slag indicated by the dip in the curve progression, which occurs at approximately 0.2 s for all three refinement levels. Since this is a two-dimensional simulation the obtained fields are based on reduced governing equations and therefore only represent the physical domain to a certain degree.

The mesh independence study on type B crucible in Fig. 6 shows similar results as described for type A. A moderate variation in the results is observable at the end of the outflow, beginning at approximately 0.8 s. A local maximum in the volume flow rate is present at 0.9 s, for which refinement level 3 yields the maximum and level 1 the minimum value with a difference of 2×10^{-6} m^3/s. Furthermore, the change in phases is represented by a sudden increase of the volume flow rate at 0.45 s. The point in time as well as the magnitude of the increase is identical for all refinement levels.

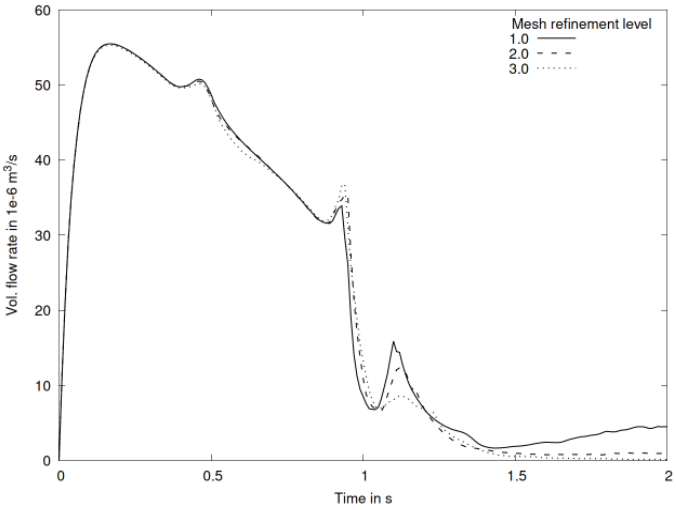

Fig. 6. Volume flow rate for the two-dimensional mesh independence study at the outlet of type B crucible during discharge for three mesh refinement levels

The following part of this section shows the numerical results of the three-dimensional cases. The average phase fraction at the outlet is displayed vs. the discharge time in Fig. 8 and 10 for two types of crucibles A and B respectively. Phase fraction of 1 correlates to a specific homogeneous phase. A decrease of one of the fluid phase fractions has to result in a corresponding increase of the opposite one. Air is excluded from the diagrams as the third fluid phase.

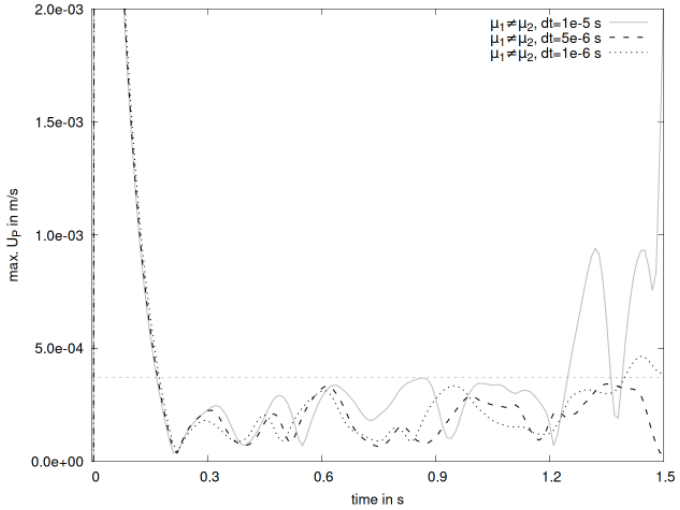

Fig. 7. Maximum parasitic currents U_P in 2D droplet case with varying thermophysical properties between slag droplet and bulk steel phase.

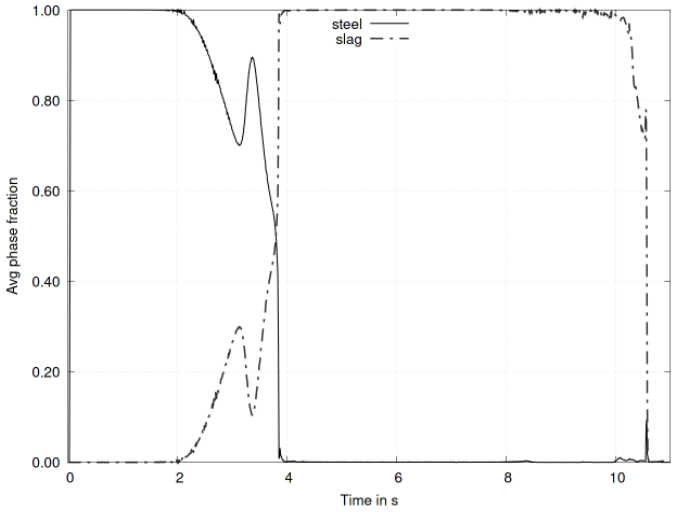

Fig. 8. Average phase fraction (steel-slag system) at the outlet of the type A crucible over the discharge time as a result of a three-dimensional numerical simulation

Numerical errors arise from the treatment of the surface force term in equation (5) by the CSF method by producing artificial velocities near the interface as a result of the balancing of forces in the Navier-Stokes equations (3). Spurious currents U_P are of small magnitude with amplitudes depending on phase properties e.g. interfacial tension and density ratio. From [2] we obtain a critical time step Δt_S in equation (11) as stability constraint during explicit treatment of the surface tension term in equation (5)

$$\Delta t_S < \left[\frac{\langle \rho \rangle (\Delta s)^3}{2\pi\sigma} \right]^{1/2} \tag{11}$$

with the mean density $\langle \rho \rangle = 0.5(\rho_1 + \rho_2)$, the interfacial tension σ and cell width Δs of an equidistant mesh. To evaluate spurious currents with the current multiphase solver and thermophysical properties, a transient 2D test case of a slag droplet in a zero-gravity environment has been set up. Slag is entrained in a bulk steel phase with a domain width of 20 mm and 150 cells in x and y-direction, a droplet diameter of 5 mm positioned at the centre of the domain yielding a critical time step of 4.02×10^{-5} s. Both phases have different thermophysical properties e.g. densities and viscosities to be conform to the 3D simulation of the crucible discharge.

As a result, parasitic currents are present at the interface of steel and slag due to the CSF method. The time step shows little to no effect on the droplet stability as the reduction of Δt_S only delays the point in time at which the droplet becomes unstable by moving away from its initial position until reaching the domain walls. Furthermore, the magnitude of spurious currents shows transient behaviour with a maximum amplitude of approximately 1.8×10^{-4} m/s for the time interval between 0.3 and 1.2 s, as shown in Fig. 7 for time steps 1×10^{-5}, 5×10^{-6} and 1×10^{-6} s for which $\Delta t < \Delta t_S$ applies.

By considering only a time interval between 0.3 and 1.2 s, we can conclude that oscillations with constant amplitude in $|U_P|$ are insignificant for the main flow of the 3D crucible outflow simulations. In a two fluid system with varying viscosities, the viscous damping capabilities of spurious currents are unequal between the phases. This may be the reason for the time dependent and increasing amplitude $|U_P|$ and for the droplet becoming unstable in a 2D zero-gravity environment.

In Fig. 9, the velocity field for the bottom part of the type A crucible is displayed. The velocity profile on the interface

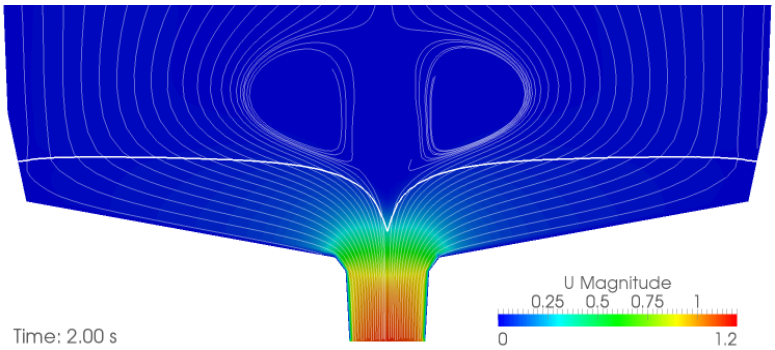

Fig. 9. Magnitude of the velocity U on a two-dimensional plane of the type A crucible outlet region at a physical time of 2.00 s including the interface between steel and slag (white line) and stream lines as a result of a three-dimensional numerical simulation

between steel and slag is heterogeneous and thus resulting in a high phase velocity above the outlet ($x = 0$ m) and nearly zero in left and right corners ($x \sim \pm R$) of the crucible. Furthermore, recirculation areas are visible in the streamlines above the outlet at $x = 0$ m of type A crucible and thus resulting in a positive velocity component at the centreline in y-direction. The steel-slag interface breaks at an approximate time of 2 s and then parallel outflow of steel and slag begins.

During the time period of 2-4 s a decrease of the steel phase fraction from unity to zero can be observed as shown in Fig. 8 and an equivalent increase occurring for the slag. The sum of both fractions is always unity during a time period of approximately two seconds, meaning that air is not present. This phenomenon is representing the parallel outflow of steel and slag during the discharge of the type A crucible. In comparison to type A, an instant decrease and a respective increase at approximately 2.1 s of the steel and slag phase fractions occurs in type B, which is shown in Fig. 10. An average phase fraction decrease from 0.23 to 0.21 during the phase change from steel to slag occurs at 2.1 s, corresponding to a diameter decrease of the fluid stream cross section.

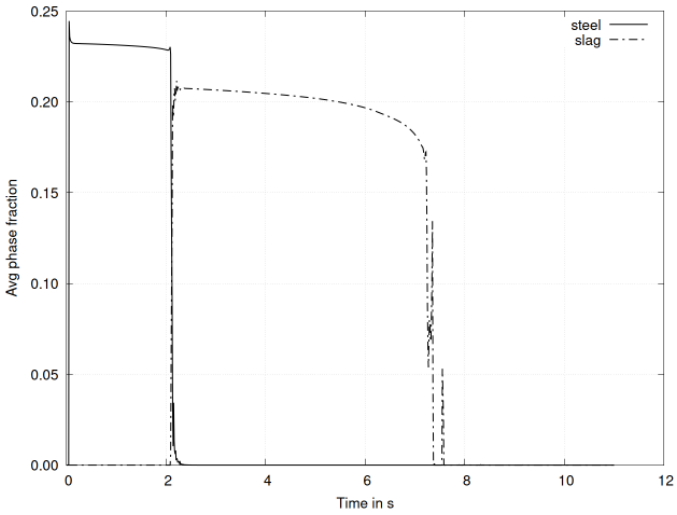

Fig. 10. Average phase fraction (steel-slag system) at the outlet of the type B crucible over the discharge time as a result of a three-dimensional numerical simulation

In Fig. 10 the overall phase fraction shows a maximum of around 0.25 and thus meaning that a part of the crucible outlet is filled with air at all times. The schematic geometry of the type B crucible is displayed in Fig. 1, showing a stepwise diameter widening at the lower end and resulting in a permanent air entrapment at the outlet. Therefore, neither the phase fraction of steel or slag can reach unity. In type B, a smooth transition during the phase change from steel to slag occurs, which can be explained by investigating the velocity field near the outlet shown in Fig. 11.

Fig. 11 shows the velocity distribution in type B crucible at time 2.05 s with the interface between steel and slag indicated by a white line. The velocity magnitude $|u|$ is homogeneously distributed along the interface for the type B crucible and thus

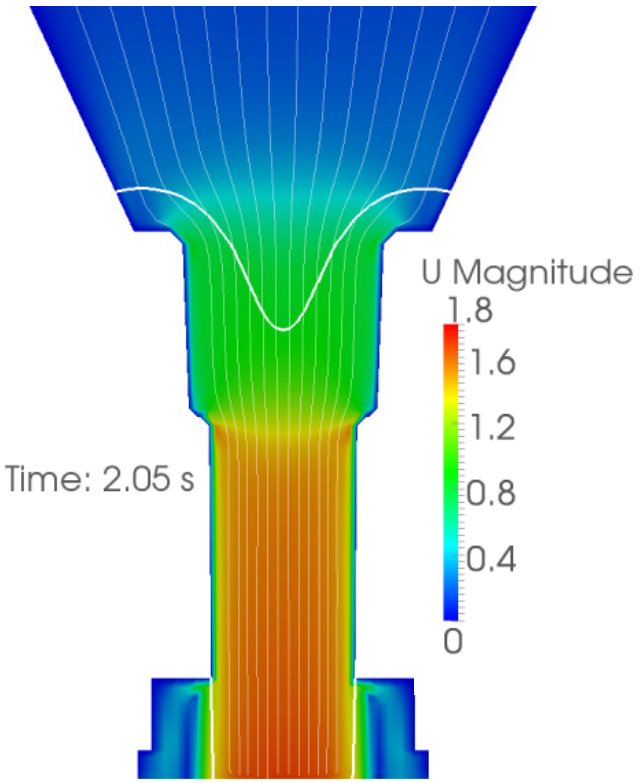

Fig. 11. Magnitude of the velocity U on a two-dimensional plane of the type B crucible outlet region at a physical time of 2.05 s including the interface between steel and slag (white line) and stream lines as a result of a three-dimensional numerical simulation

meaning that no steel volume is being held back during the end of the outflow.

8. Discussion and conclusion

As we compare the numerical results of the type A crucible for two different multiphase systems, namely water-oil and steel-slag in Fig. 3 and 8 respectively, the influence of the thermophysical properties can be seen in the extent of the time interval of the concurrently proceeding binary outflow of both liquid phases. In the water-oil system the parallel outflow of water and oil lasts about 4 s and in the steel-slag system the critical outflow takes only half the time.

The interfacial tension of the steel-slag system is approximately 15 times higher and this results in a shorter time period for the parallel outflow of the two liquid phases since the secondary phase has to overcome a higher interfacial force compared to the water-rapeseed oil system.

The main reason for the breakthrough and parallel outflow is the heterogeneous velocity field above the outlet of the crucible. By comparing the two crucibles from Fig. 1, one can estimate that local velocities in the corner area at $x \sim \pm R$ of type A crucible are nearly zero. Above the outlet at $x = 0$ m however, a high velocity in negative y-direction is dominant and therefore resulting in an increased interface velocity compared to the corner area at $x \sim \pm R$ of the crucible.

In section 6, the VOF solver *multiphaseInterFoam* has been successfully validated against experimental data from a water-rapeseed oil crucible discharge. It is not certain if the concurrently proceeding outflow of two liquid phases is also occurring in the steel-slag-air multiphase system. The numerical results and the internal crucible geometry indicate such behaviour however. Temperatures above 2000°C complicate any experimental investigation of the steel-slag-air system in its liquid state. A parallel outflow of steel and slag could certainly reduce the quality of a weld. However, precautions have been taken to impede the slag from entering the welding gap by letting steel and slag separate before flowing downwards into the gap.

Acknowledgement

The author appreciates the opportunity of investigating this topic in the field of multiphase systems and the aluminothermic welding process as well as the assistance during the planning and realization of the experiments.

REFERENCES

[1] M. Bielnicki, J. Jowsa, A. Cwudziński, Arch. Metall. Mater. **60**, 257-262 (2015).

[2] J.U. Brackbill, D.B. Kothe, C.A. Zemach, J. Comput. Phys. **100** (2), 335-354 (1992).

[3] Y. Chung, A.W. Cramb, Metall. Mater. Trans. B **31B**, 957-971 (2000).

[4] S. Márquez Damián, An Extended Mixture Model for the Simultaneous Treatment of Short and Long Scale Interfaces, PhD Thesis, Universidad Nacional Del Litoral, Santa Fe, 2013.

[5] D. Ghosh, V.A. Krishnamurthy, S.R. Sankaranarayanan, J. Min. Metall. Sect. B-Metall. **46**, 41-49 (2010).

[6] L.A. Girifalco, R.J. Good: J. Chem. Phys. **61**, 904 (1957).

[7] Firma Th. Goldschmidt, Verfahren zur Herstellung von Metallen oder Metalloiden oder Legierungen derselben, Kaiserliches Patentamt Berlin Nr. 96317 (1898).

[8] M.B. Goldschmit, S.P. Ferro, H.C. Owen, Prog. Comput. Fluid Dy. **4**, 12-19 (2004).

[9] R. Hagemann, R. Schwarze, H.P. Heller, P.R. Scheller, Metall. Mater. Trans. **B 44** (1), 80-90 (2013).

[10] C.W. Hirt, C.D. Nichols, J. Comput. Phys. **39**, 201-225 (1981).

[11] X. Huang, B.G. Thomas, Can. Metall. Quart. **37**, 197-212 (1998).

[12] J. Iwanciw, K. Pytel, E. Kawecka-Cebula, M. Kostołowska, Arch. Metall. Mater. **53** (2), 575-581 (2008).

[13] S. Pirker, Steel Res. Int. **81** (8), 623-629 (2010).

[14] H. Rusche, Computational Fluid Dynamics of Dispersed Two-Phase Flows at High Phase Fractions. PhD thesis, Imperial College of Science, Technology & Medicine, London, 2002.

[15] R. Sankaranarayanan, R.I.L. Guthrie, Ironmak. Steelmak. **29**, 147-153 (2002).

[16] P. Scheller, R. Hagemann, Arch. Metall. Mater. **57** (1), 283-289 (2012).

[17] P. Sulasalmi, A. Kärnä, T. Fabritius, J. Savolainen, ISIJ Int. **49** (11), 1661-1667 (2009).

[18] C. Xuan, H. Shibata, S. Sukenaga, P. Jönsson, K. Nakajima, ISIJ Int. **55** (9), 1882-1890 (2015).

[19] S. Zalesak, J. Comput. Phys. **31**, 335-362 (1979).